English

前言

会议机构

报告人介绍

关肇直奖

张贴论文奖

论文目录

全文搜索

作者索引

IEEE Catalog Number: CFP1940A-USB
ISBN: 978-988-15639-6-5

2019 Chinese Control Conference

Proceedings of the 38th CCC

第三十八届中国控制会议论文集

Technical Committee on Control Theory

主办单位：中国自动化学会控制理论专业委员会
中国自动化学会
中国系统工程学会
承办单位：广东工业大学
协办单位：中国科学院数学与系统科学研究院
中国工业与应用数学学会
华南理工大学
广东省自动化学会
亚洲控制学会
IEEE控制系统协会
韩国控制、机器人与系统学会
日本仪器与控制工程师学会

2019年7月27-30日　中国·广州

Proceedings of the 38th Chinese Control Conference
July 27-30, 2019, Guangzhou, China

Research on MAV Indoor Localization and Yaw Estimation Algorithm Based on Onboard Ultrasonic Sensors

Xiaoke Feng[1], Lingyu Yang[1], Jing Zhang[1], Yuhan Mou[1]

1. Beihang University (Beijing University of Aeronautics and Astronautics), Beijing 100191, Beijing 100190
E-mail: 18580530093@163.com;yanglingyu@buaa.edu.cn;zhangjing2013@buaa.edu.cn; mouyh@buaa.edu.cn

Abstract: Because of the lack of GPS signal and strong magnetic field interference in indoor environment, the indoor localization of micro aerial vehicle(MAV)is a challenging problem in practice. In this paper, an MAV indoor positioning algorithm is proposed, which does not rely on magnetic compass and GPS. The improved unscented Kalman filter (UKF) algorithm is used to fuse the information only four ultrasonic sensors and the Inertial Measurement Unit carried by the drone itself to localize in the indoor environment with a prior map. This method does not rely on magnetic compass, so it greatly reduces the impact of indoor electromagnetic environment on localization. Results from simulation demonstrates the effectiveness of the proposed algorithm.

Key Words: MAV, indoor localization, ultrasonic sensors, IMU, prior map, UKF

1 Introduction

High precision localization is one of the keys for MAV to fly indoors and perform complex tasks. On the one hand, it needs to the localize the MAV in GPS-denied environments, on the other hand, complex indoor electromagnetic environment significantly reduces the performance of magnetic compass sensors, and directly affects indoor navigation and localization. For the Micro Aerial Vehicle (MAV), the problem becomes more complicated due to the strict restrictions on its size, load and computational capacity.

Currently, the commonly used sensors for indoor localization include onboard sensors and off-board sensors. The on board sensors include IMU, laser range finder[1] (LRF), monocolar/stereo/ominidirection camera[2], depth camera[3], ultrasonic[4], infrared range finder[5], etc. the off-board sensors require the assistance of external devices, such as bacons or wireless signal sources. Typical off-board sensors include UWB[6], WIFI[7], RFID[8], Bluetooth and so on.

IMU is one of the essential basic onboard sensor, and mainly includes micro accelerometers and gyroscopes, providing pose measurement. However, without external correction, errors of gyroscopes and accelerometers will be accumulated via the integral calculations. As a result, localization error of the inertial navigation system will increase gradually after long-time operation[9].Therefore, how to combine the IMU and other types of sensors and improve the localizing accuracy has become an urgent problem to solve.

The off-board sensors are suitable for an familiar environment since it has to prearrange some equipment in the environment. By contrast, onboard sensors are more robust to the environment. Among some wildly used inboard sensors, ultrasonic sensors have advantages of small volume, low cost, nearly free from environmental impact, the direct way to obtain distance information, and low data processing complexity, so it is suitable for a MAV platform with small size and light load[10]. Therefore, in this paper, the ultrasonic is chosen to localize the MAV.

The distance calculated by ultrasonic sensors is based on the propagation speed of the ultrasonic waves and the time when the sonar transmitter emits and receiver receives the ultrasonic waves reflected from the obstacle surface. The existing MAV localization algorithm equipped with ultrasonic as on-board sensors generally requires an accurate yaw angle[10][11][12]. In real indoor environment, external factors have a large influence on the magnetic field, causing large interference to the measurement of the magnetic compass. In paper[10] and[11], the premise of accurate localization is that the magnetic compass can accurately measure the yaw angle, in paper[12],a known and constant yaw angle guarantee accurate localization.

This paper proposes an improved Unscented Kalman Filter (UKF) based indoor locating algorithm, which aims to solve the uncertainty of yaw angle in indoor localization. There are various kinds of interference in indoor environment, which have a great influence on the distribution of the magnetic field in the room. If the yaw angle is measured only by magnetic compass, the accuracy of the locating algorithm will greatly reduce. An improved UKF is presented in this paper to estimate the yaw angle and correct the absolute localization with ultrasonic measurement, enhancing the robustness of the algorithm.

Other parts of this paper are as follows: the second section introduces the MAV platform and ultrasonic characteristics. In the third section, the MAV system is modeled to obtain its motion equation. The fourth section introduces steps of the improving UKF localization algorithm. In the fifth section, a simulation verification experiment is carried out to verify the effectiveness of the proposed algorithm in locating and yawing angle estimation in a barrier-free enclosure space.

2 Micro Aerial Vehicle Platform

2.1 Micro Aerial Vehicle

The MAV used in this paper adopts the "X" type layout, and four ultrasonic are installed along the positive and

negative directions of the body axis for localization, as shown in Fig 1.

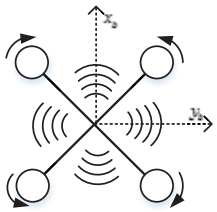

Fig 1 Body coordinate of MAV

Fig 2 shows the fuselage of the MAV. The whole fuselage with ultrasonic sensors weighs about 75g and the wheelbase is 15cm. MPU6000 is used as the triaxial accelerometer and LSM303D is used as the triaxial magnetometer. The data sampling period of both sensor is about 8ms.The flight control part follows the open source PX4 project, and various tasks of flight control are managed and scheduled by operating system. Moreover, it is easy to develop a customized flight control missions, which can easily store and handle all kinds of data during the flight of MAV.

Fig 2 The MAV platform

2.2 Ultrasonic Module

Four MB1222 ultrasonic sensors are installed on the bottom of the MAV, and the angle between adjacent ultrasonic directions is 90°, respectively measuring distance of the four directions. MB1222 is a single-probe ultrasonic sensor with a diameter of about 1.5cm and a net weight of about 8g, as shown in Fig 3.

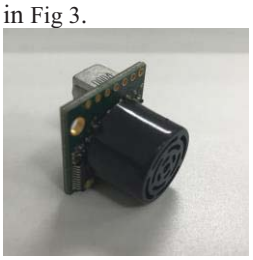

Fig 3 MB1222 ultrasonic module

The principle of ultrasonic distance measurement is that the ultrasonic sensor transmit a series of ultrasonic waves and receive the ultrasonic signal reflected back from the obstacle and calculate the time difference between transition and reception. The range of ultrasonic transmission is determined by the lobe[13]. As long as an obstacle is in the ultrasonic lobe area and the reflected signal is detected by the receiver, the distance between the obstacle and the transmitting point can be calculated. By placing a dam-board in front of the ultrasonic sensor and constantly moving the board, the left and right sides boundary of MB1222 is determined [13]. Taking the origin as the transmitting point of ultrasonic wave, the abscissa is the x_s axis of ultrasonic wave, which represents the longitudinal distance, and the ordinate is y_s lateral distance, so the beam pattern of ultrasonic wave is shown in Fig 4.

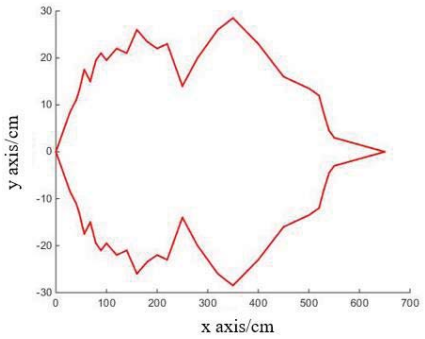

Fig 4 Beam pattern of MB1222

According to the conclusion in literature [13], in order to simplify calculation, the beam pattern can be simplified to a multi-ray model by connecting the boundary points on the contour with the ultrasonic transmitting point.

The simplified multi-ray model of MB1222 is shown in Fig 5.

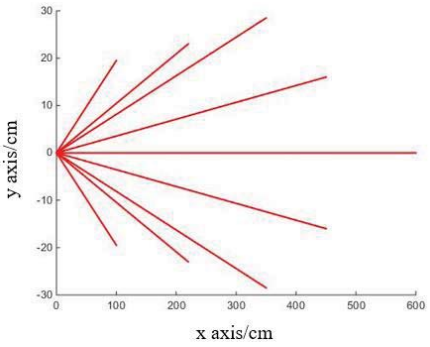

Fig 5 Ray model of ultrasonic

Take the ultrasonic transmitting point $\mathbf{s}_0$ as the starting point of the line segment, and $\mathbf{s}_1,\mathbf{s}_2,\cdots\mathbf{s}_j,\cdots\mathbf{s}_k$ represent the end point of the line segments, where $\mathbf{S}_j$ represents the j^{th} ray of the ultrasonic wave. Then the ray model of ultrasonic wave can be expressed as

$$\begin{cases}\mathcal{S}=\ \mathbf{S}_0,\mathbf{S}_1,\mathbf{S}_2,\ldots,\mathbf{S}_k \\ \mathbf{S}_1=\overline{\mathbf{s}_0\mathbf{s}_1},\mathbf{S}_2=\overline{\mathbf{s}_0\mathbf{s}_2},\ldots,\mathbf{S}_k=\overline{\mathbf{s}_0\mathbf{s}_k},\end{cases} \tag{1}$$

Calculating the theoretical distance of ultrasonic wave to the wall can be simplified as calculating the intersection points of the ultrasonic rays and the wall. Set the wall as $\mathcal{M}$, if the ultrasonic multi-ray model intersects with the wall, record the intersection point as

$$\mathcal{R}=\ \mathbf{r}_1,\mathbf{r}_2,\cdots\mathbf{r}_q\ =\mathcal{S}\otimes\mathcal{M} \tag{2}$$

Take the minimum distance as the measurement result, the theoretical measurement of the ultrasonic l is given by

$$l=\begin{cases}\min\limits_{\mathbf{r}_i}\ \left\|\mathbf{r}_i-\mathbf{s}_0\right\|_2 & \mathcal{R}\neq\varnothing \\ l_{\max} & \mathcal{R}=\varnothing\end{cases} \tag{3}$$

Where $l_{\max}$ is predefined value if $\mathcal{S}$ and $\mathcal{M}$ do not have an intersection.

3 Modeling of MAV Indoor localization system

Before systems modeling, two coordinates are defined:

Map coordinate (Ground coordinate) $O-x_my_mz_m$: North East Down coordinate.

Body axis system $O-x_b y_b z_b$: the origin is fixed to the center of gravity of the quadrotor, and the direction of x_b axis and y_b axis is shown in Fig 6.

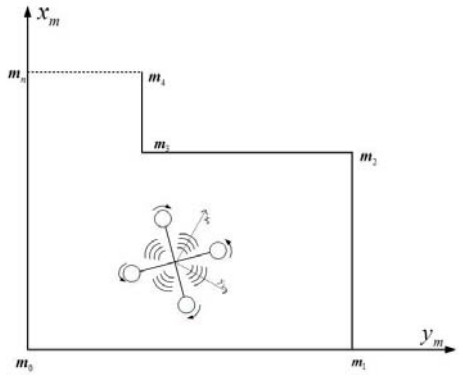

Fig 6 Presentation of prior map

The representation method of prior map is to extract the inflection points in real map, and the wall between each inflection is assumed to be straight. As shown in Fig 6, $\boldsymbol{m}_i$ represents the coordinate of the i^{th} inflection point, and the coordinates of all inflection points in the map are written as a matrix $\boldsymbol{M} \in R^{2\times n}$ with the origin being the starting point and ranging in a counterclockwise direction.

Assuming that the MAV only moves in a two-dimensional plane, and its yaw angle acceleration in the map coordinate system is the angular acceleration measured by gyroscope.

The state variable of the system is $\mathbf{X}=[P_{m_x}, v_{m_x}, P_{m_y}, v_{m_y}, \psi]^T$, and the subscript m indicates that the variable is defined in the ground coordinate. Where P_{m_x} is the direction of the MAV O-x_m while v_{xm} is the velocity, and P_{m_y} is the direction O-y_m , while v_{ym} is the velocity; ψ is the yaw angle of the MAV, and in 2-D plane, and it is defined as the angle between the O-x_m and O-x_b .

The input of the system is defined as $\mathbf{u}=[a_x \quad a_y \quad \omega_z]^T$, where ω_z is the yaw angular velocity, a_x and a_y are the acceleration in the body frame

The state equation of the system is shown in eq. (4).

$$\begin{cases} x_m(k+1) = x_m(k) + v_{xm}(k)T_A + \frac{1}{2}[a_x \cos\psi(k) - a_y \sin\psi(k)]T_A^2 + w_1 \\ v_{xm}(k+1) = v_{xm}(k) + [a_x \cos\psi(k) - a_y \sin\psi(k)]T_A + w_2 \\ y_m(k+1) = y_m(k) + v_{ym}(k)T_A + \frac{1}{2}[a_x \sin\psi(k) + a_y \cos\psi(k)]T_A^2 + w_3 \\ v_{ym}(k+1) = v_{ym}(k) + [a_x \sin\psi(k) + a_y \cos\psi(k)]T_A + w_4 \\ \psi(k+1) = \psi(k) + \omega_z T_A + w_5 \end{cases} \quad (4)$$

where $w_1 - w_5$ are the zero mean white noise. T_A is the sampling period of the accelerometer and the gyroscope.

The above equation of state can be simplified to

$$\mathbf{X}(k+1) = f(\mathbf{X}(k), \mathbf{u}) + \mathbf{W}(k) \quad (5)$$

where $\mathbf{W}(k)=[w_1, w_2, w_3, w_4, w_5]$ is the zero mean white noise.

The observation variable of the system is the measurement of four ultrasonic sensors. According to the MAV's location, ray model and prior map information, the ultrasonic theoretical measurements can be calculated, and by

$$\boldsymbol{l}(k) = h(P_{mx}(k), P_{my}(k), \psi(k), \boldsymbol{M}, \boldsymbol{S}) \quad (6)$$

Where $(P_{mx}(k), P_{my}(k))$ is the position in prior map $\boldsymbol{M}$, $\boldsymbol{S}$ is the model of ultrasonic. The observation equation is a nonlinear function.

4 Indoor positioning algorithm based on improved UKF

On the basis of the MAV kinetic model, this paper adopts the kalman filter to estimate the MAV's indoor localization.

When the state equation and the observation equation are linear, the linear kalman filter can be used. However, in the MAV's motion model established in the previous section, both the measurement equation and the observation equation are nonlinear, the commonly used methods for the state estimation of the nonlinear system are Extended Kalman Filter (EKF) and Unscented Kalman Filter (UKF).

Different from EKF which transfer nonlinear functions to linear functions, UKF adopts of unscented transformation (UT) in the one-step estimation equation to deal with the mean and covariance of the nonlinear transfer problem rather than calculate Jacobi matrix. UT approximate the nonlinear function through the probability distribution of sample points. For the case where both the equation of state and the observation are nonlinear, UKF needs UT twice at the state estimation and observation estimation. In general, UKF adopts the same UT parameters for the selection of sampling points in the two estimation. Considering the particularity of the observation equation, if sampling points distribute in a large range, observation might jump or even be beyond the map leading to invalid observation. Therefore, the UKF algorithm is improved in this paper. In two UT transformations, different sampling parameters are used respectively to control the sampling range of state estimation and observation estimation so as to obtain more accurate mean and covariance.

Besides, because yaw angle is the state variable, the angular velocity measured by gyroscope is set as input, and the ultrasonic measurement is set as the observed variable to estimate the yaw angle.

The improved UKF algorithm steps are as follows.

1、 Set initial state

Set the accelerometer and gyroscope sampling period as T_A , the ultrasonic sampling time period as T_s ; the variance

of the state noise as Q, the observed noise variance as R and set the initial $P(0|0)$.

Set the parameters in the UT twice:

Since the state equation and the observation equation in this paper are both nonlinear, in conventional UKF algorithm, unscented transformation are required twice, where UT transform parameters are the same. In this paper, due to the discontinuity of the observation equation, to decrease the sampling range in UT transform, therefore, the two UT transform parameters are different to achieve a better estimation effect. The parameters determining the value of the weight, including α, β and λ, where λ is calculated according α, n and κ.

Different subscripts indicate difference sampling parameters in two unscented transformations. Set α_1 as a small positive number. Usually $10^{-4} \le \alpha_1 \le 1$. β_1 relates to the distribution of state variables $\mathbf{X}$, and if $\mathbf{X}$ is normal distribution, the optimal value of β_1 is 2. $\lambda_1 = \alpha_1^2 (n+\kappa_1) - n_1$, where n_1 is the dimension of the state variable, generally $\kappa_1 = 3 - n_1$.

α_2 could be different from to α_1, and can be adjusted according to the range of sampling points. β_2 equals to β_1, $\lambda_2 = \alpha_2^2 (n+\kappa_2) - n_2$ where $\kappa_2 = 3 - n_2$ and n_2 is the dimension of the observed variable.

2、 Generate $2n+1$ sample points at time k

$$\hat{X}(k|k)^{(0)} = \hat{X}(k|k) \tag{7}$$

$$\hat{X}(k|k)^{(i)} = \hat{X}(k|k)^{(0)} + (\sqrt{(n+\lambda_1)P(k|k)})_{(i)} \quad (i = 1, \cdots n) \tag{8}$$

$$\hat{X}(k|k)^{(i)} = \hat{X}(k|k)^{(0)} - (\sqrt{(n+\lambda_1)P(k|k)})_{(i-n)} \quad (i = n+1, \cdots 2n) \tag{9}$$

3、 Calculate the 2n+1 one-step sampling estimated state variables at time k

$$\hat{X}(k+1|k)^{(i)} = f[X(k|k)^{(i)}, u(k)] \tag{10}$$

$$\hat{X}(k+1|k) = \sum_{i=0}^{2n} W_i^{(m)}(1) X(1)(k+1|k)^{(i)} \tag{11}$$

where the weight of each state sample point is

$$W_0^{(m)}(1) = \frac{\lambda_1}{n+\lambda_1} \tag{12}$$

$$W_i^{(m)}(1) = \frac{1}{2(n+\lambda_1)} \quad (i = 1, \cdots, 2n) \tag{13}$$

4、 Calculate $P(k+1|k)$

$$P(k+1|k) = \sum_{i=0}^{2n} W_i^{(c)}(1) \bullet [\hat{X}(k+1|k)^{(i)} - \hat{X}(k+1|k)] \bullet [\hat{X}(k+1|k)^{(i)} - \hat{X}(k+1|k)]^T + Q \tag{14}$$

where, the weight of each sample point is

$$W_0^{(c)}(1) = \frac{\lambda_1}{2n+\lambda_1} + 1 - \alpha_1^2 + \beta_1 \tag{15}$$

$$W_i^{(c)}(1) = \frac{1}{2(2n+\lambda_1)} \quad (i = 1, \cdots 2n) \tag{16}$$

5、 If observation of ultrasonic update, calculate 2n+1 observed one-step sampling estimated variables

$$\hat{X}(k+1|k)^{(0)} = \hat{X}(k+1|k) \tag{17}$$

$$\hat{X}(k+1|k)^{(i)} = \hat{X}(k+1|k)^{(0)} + (\sqrt{(n+\lambda)P(k+1|k)})_{(i)} \tag{18}$$

$$(i = 1, \cdots n)$$

$$\hat{X}(k+1|k)^{(i)} = \hat{X}(k+1|k)^{(0)} - (\sqrt{(n+\lambda)P(k+1|k)})_{(i-n)} \tag{19}$$

$$(i = n+1, \cdots 2n)$$

6、 Calculate the observed estimated variables at time k+1

$$\hat{Z}(k+1|k)^{(i)} = h[\hat{X}(k+1|k)^{(i)}] \tag{20}$$

$$\hat{Z}(k+1|k) = \sum_{i=0}^{2n} W_i^{(m)}(2) \hat{Z}(k+1|k)^{(i)} \tag{21}$$

where, the weight of each sample point is

$$W_0^{(m)}(2) = \frac{\lambda_2}{n+\lambda_2} \tag{22}$$

$$W_i^{(m)}(2) = \frac{1}{2(n+\lambda_2)} (i = 1, \cdots 2n) \tag{23}$$

7、 Calculate $P_{xz}(k+1|k)$ and $P_{zz}(k+1|k)$

$$P_{xz}(k+1|k) = \sum_{i=0}^{2n} W_i^{(c)}(2) \bullet [X(k+1|k)^{(i)} - \hat{X}(k+1|k)] \bullet [Z(k+1|k)^{(i)} - \hat{Z}(k+1|k)]^T \tag{24}$$

$$P_{zz}(k+1|k) = \sum_{i=0}^{2n} W_i^{(c)}(2) \bullet [Z(k+1|k)^{(i)} - \hat{Z}(k+1|k)] \bullet [Z(k+1|k)^{(i)} - \hat{Z}(k+1|k)]^T \tag{25}$$

where, the weight of each sample point is

$$W_0^{(c)}(2) = \frac{\lambda_2}{2n+\lambda_2} + 1 - \alpha_2^2 + \beta_2 \tag{26}$$

$$W_i^{(c)}(2) = \frac{1}{2(2n+\lambda_2)} \quad (i = 1, \cdots 2n) \tag{27}$$

8、 Calculated gain matrix

$$K(k+1) = P_{xz}(k+1|k) P_{zz}^{-1}(k+1|k) \tag{28}$$

9、 Calculated final filter value

$$\hat{X}(k+1|k+1) = \hat{X}(k+1|k) + K(k+1)[Z(k+1) - \hat{Z}(k+1|k)] \tag{29}$$

$$P(k+1|k+1) = P(k+1|k) - K(k) P_{zz}(k+1|k) K^T(k+1) \tag{30}$$

All the necessary equations above for improved UKF have been derived. Because the sampling period of accelerometer and gyroscope and sampling period of ultrasonic is different, and the accelerometer and gyroscope sampling period is 8 ms, and ultrasonic sampling period is 200 ms, the sampling frequency of the accelerometer is far higher than that of ultrasonic, as a result, the strategy is to iterate the position of the MAV via accelerometer and its variance when ultrasonic has no new measurement as eq.(5). Since there is no measurement update, the result of observation update is directly taken as the filtering result of UKF, as eq.(31)

$$\begin{cases} \hat{\boldsymbol{X}}(k+1|k+1) = \hat{\boldsymbol{X}}(k+1|k) \\ \boldsymbol{P}(k+1|k+1) = \boldsymbol{P}(k+1|k) \end{cases} \tag{31}$$

When the ultrasonic obtains new data, the estimated value of the accelerometer is corrected by the ultrasonic measurement as eq.(29).

In addition, because eq.(6) is an nonlinear discontinuous function, in some special positions in the map, the ultrasonic measurement may occur jumps, as shown in Fig 7, which will have an effect on the localization algorithm. The reason is that there is an error between the predicted localization and the actual localization, and the observation equation is discontinuous. Extracting the actual observation and prediction of the points near the jump points to compare the ultrasonic measurements, it is found that the jump do exist.

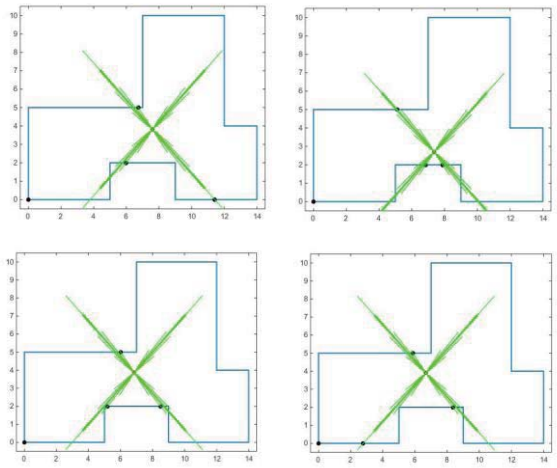

Fig 7 Ultrasonic measurement jump examples

There are a group of intersection points between the ultrasonic ray model and the wall, and the black point in Fig 7 represents the intersection point with the shortest distance. The shortest distance from the intersection point to the origin is taken as the theoretical measurement of the ultrasonic. The reason for the jump is that the ultrasonic measured the edge of a wall at the last moment, and then measured the distance to the other wall at the next moment due to the change of position, as a result the jump of the measurement occurres.

In the case where there is a large jump of sensor measurement, although the measurement variance increases reducing kalman gain, observation data with obvious errors are still fused. After iteration, the fusion accuracy decreases. Therefore, the validity of the measurement should be verified after the measurement update. The method to check the validity of data is residual chi-square test.

Residual chi-square test is a statistical hypothesis test that determines whether a fault has taken place by checking whether the mean and variance of a constructed n-dimensional Gaussian distribution random vector are consistent with the assumed value. If not, it can be inferred that a fault has occurred. This method has been widely used in fault detection of integrated navigation systems[14][15].

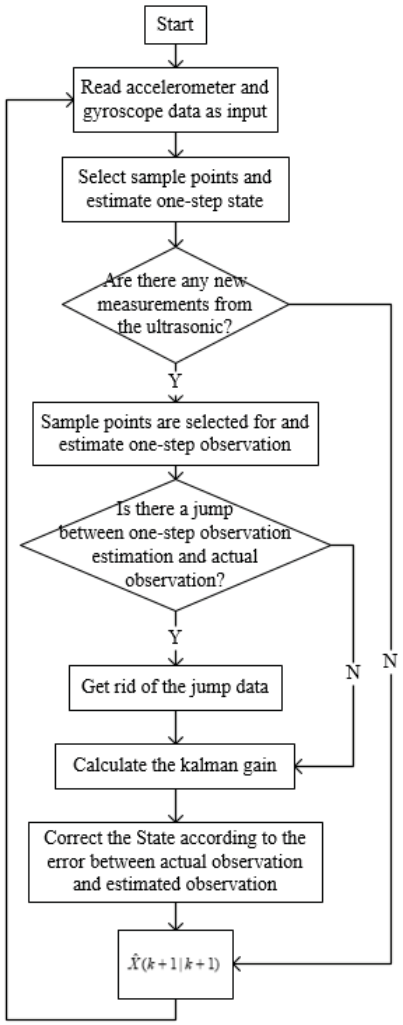

Fig 8 Localization algorithm flow chart

As for UKF, the predicted observation residual array is

$$e_k = Z_k - \hat{Z}_{k|k-1} \tag{32}$$

The corresponding covariance matrix is

$$P_{e_k} = \sum_{i=0}^{L-1} W_c^i (Z_{k|k-1}^i - \hat{Z}_{k|k-1})(Z_{k|k-1}^i - \hat{Z}_{k|k-1})^T + R_k \tag{33}$$

where Z_k is the actual measurement; $Z_{k|k-1}^i$ is the i th estimated observation array according to the i th sampling points, $\hat{Z}_{k|k-1}$ is the estimated observation array, and W_c^i is the weighted used for covariance weighting; R_k is the measurement noise variance matrix.

If there is no jump, e_k is zero mean gaussian white noise, however, if there is a jump, the residuals isn't zero gaussian white noise anymore.

The chi-square test function is defined as

$$\lambda_k = e_k^T P_{e_k}^{-1} e_k \tag{34}$$

The function subject to chi-square distribution of L degrees of freedom and L is the dimension of observation vector. Therefore, the criterion that whether a jump of happen is

$$\begin{cases} \lambda_k > T_D & jump \\ \lambda_k \le T_D & no\ jump \end{cases} \tag{35}$$

In eq. (35), T_D is the preset threshold, which can be determined by the preset false alarm rate.

There are 4 observed variables in observation equation, when there is jump of measurement, not all of them are invalid, and only valid observations are kept. Therefore, the chi-square test with dimension 1 is conducted on the 4 observation to remove the correction of the observation which exceeds the preset threshold. That is to set the row of kalman gain to zero, which correspond to the order of invalid observations.

Flow chart of the algorithm is shown in Fig 8.

5 Simulation result

In this section, the localization algorithm proposed above is simulated and verified. Firstly, a polygon prior map $\boldsymbol{M}$ without obstacles is set. Simulation steps T_A is known, as well as acceleration data and yaw acceleration data driving the aircraft $\mathbf{u}$. The initial state of the MAV is set as

$$\mathbf{X}(0)=[P_{m_x}(0)\quad v_{m_x}(0)\quad P_{m_y}(0)\quad v_{m_y}(0)\quad \psi(0)]^T$$
$$=[1\quad 0.05\quad 1\quad 0.05\quad 0.785]^T$$

According to the motion equation in section 3, the flight path of a MAV can be obtained, as shown in Fig 9.The true yaw angle of the MAV is shown in Fig 10.

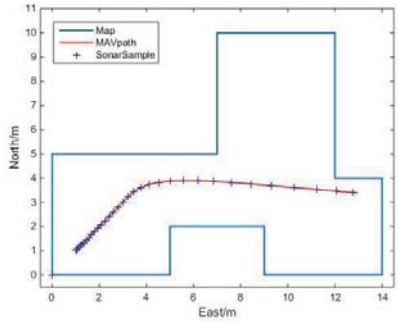

Fig 9 True trajectory of MAV

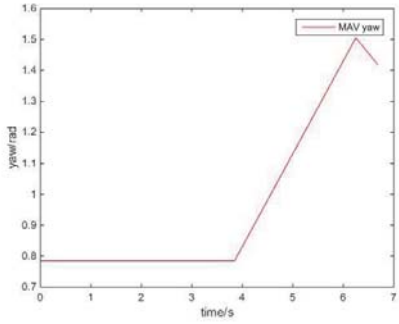

Fig 10 True yaw angle of the MAV

The curve in Fig 9 is the flight path of the MAV, and the point with "+" corresponds to the sampling point of the ultrasonic sensors. The flight path in Fig 9 is the actual path of the MAV. Add certain variance white noise to input data of corresponding trajectory in Fig 9, as shown in equation (37).

$$\mathbf{u}=\begin{bmatrix}a_x\\a_y\\\omega_z\end{bmatrix}=\begin{bmatrix}a_{x0}+\varepsilon_1\\a_{y0}+\varepsilon_2\\\omega_{z0}+\varepsilon_3\end{bmatrix} \tag{36}$$

where, a_{x0} is the true acceleration in direction x_b and a_{y0} is the true acceleration in direction y_b. ω_{z0} is the true value of yaw angular velocity; ε_1 and ε_2 are the white noise of the accelerometer measured in flight of the MAV, and ε_3 is the zero-offset noise which conforms to real gyroscope offset, whose unit is $(\mathrm{rad}/s)^2$.

In anywhere in the map, if the location, yaw angle, maps and ultrasonic model is known, theory measurement of ultrasonic in this location l_0 can be calculated, then noise ε_l which conforms to the actual ultrasonic noise is added to ultrasonic measurements as sampling measurements in localization algorithm, as eq.(37) shows.

$$l=l_0+\varepsilon_l \tag{37}$$

Table 1 are some simulation parameters used in the algorithm.

Table 1 simulation parameters in simulation

T_A (ms)	T_S (ms)	Q	R
8	200	diag([1,0.2,1, 0.2,0.1]^T)	0.007diag([1,1,1,1]^T)
var ε_1	var ε_2	var ε_3	var ε_l
2.2	2.2	0.06	0.007

In table 1, T_A is the sampling period of accelerometer and T_S represent the sampling period of ultrasonic, ε_1 and ε_2 are measurement noise variance of accelerometer while and ε_3 is measurement noise variance of gyroscope, and var ε_l represent measurement noise variance of ultrasonic.

Comparison is made in the following aspects:

1、Estimated location using accelerometer only

2、Estimated location and yaw angle using conventional UKF，where $\alpha_1=\alpha_2$, $\beta_1=\beta_2$, $\lambda_1=\lambda_2$.

3、Estimated location and yaw angle using improved UKF without verifying the validity of observation， where $\alpha_1\neq\alpha_2$, $\beta_1=\beta_2$, $\lambda_1\neq\lambda_2$.

4、Estimated location and yaw angle using improved UKF with verifying the validity of observation, where $\alpha_1\neq\alpha_2$, $\beta_1=\beta_2$, $\lambda_1\neq\lambda_2$.

Fig 11 shows the localization effect using only accelerometer. The noise of the accelerometer generate a large drift, leading to a large deviation in location result.

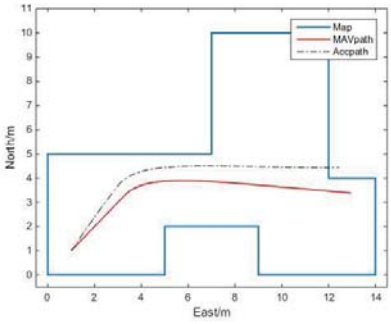

Fig 11 Localization result with only accelerometer

Fig 12 shows the localization result of conventional UKF in the same simulation conditions, where $\alpha_1=\alpha_2$, $\beta_1=\beta_2$, $\lambda_1=\lambda_2$. Fig 13 shows the comparison between conventional UKF localization error and accelerometer localization error. The path estimated by conventional UKF positioning has a large lag, and the error has exceeded the error by accelerometer.

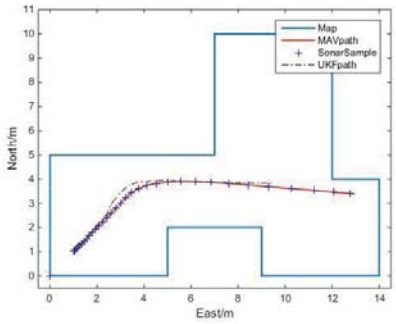

Fig 12 localization effect with conventional UKF

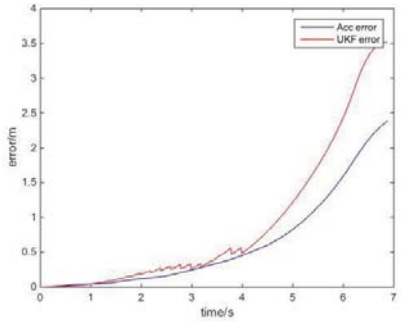

Fig 13 comparison of localization error with conventional UKF and with only accelerometer

The simulation results using the improved UKF algorithm are shown in Fig 14 and Fig 15. Fig 14 shows the result of UKF without verifying the validity of observation.

However, there is an obvious error in Fig 14 at the points where the observation jumps, which still leads to a large localization error after the jump. At the same time, the estimation accuracy of yaw angle jump, resulting in a large error, as shown in Fig 15.

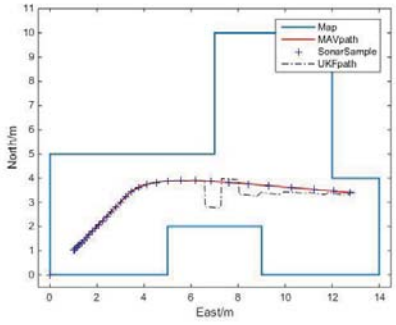

Fig 14 Localization result using improved UKF without verifying the validity of observation

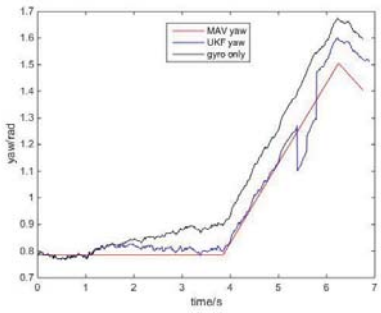

Fig 15 Yaw angle estimation result using improved UKF without verifying the validity of observation

Fig. 16 shows the filtering results after verifying the validity of observation. As the simulation results shows, the localization result could be more accurate, indicating that verifying the validity of data greatly improves the accuracy of the filtering result. In Fig. 16, when the ultrasonic measurement are updated, the position of the MAV is corrected by ultrasonic, thus improving the localization accuracy, as the dotted line shows.

Figure 17 shows the comparison of localization distance error between the localization error of improved UKF and that of accelerometer only. It is clear that the localization distance error of the accelerometer becomes larger with time due to the accumulation of accelerometer offset, while the error of UKF decreases through ultrasonic correction.

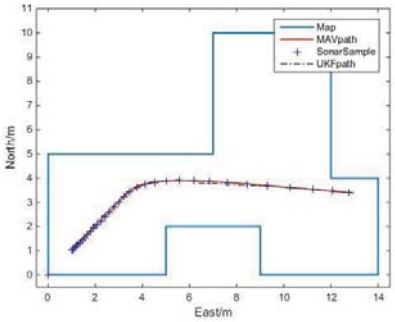

Fig 16 localization result using improved UKF with verifying the validity of observation

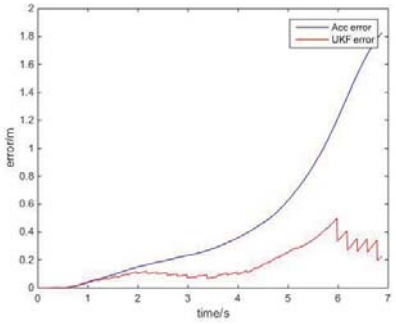

Fig 17 comparison of localization error with improved UKF and with only accelerometer

After plenty of simulations, the errors of the accelerometer localization and the UKF localization are compared, and the error statistics of the two algorithms are shown in table 2.

Table 2 comparison of localization error between two algorithms

Average localization error by accelerometer (m)	Average localization error by UKF (m)	Max localization error by accelerometer (m)	Max localization error by UKF (m)
0.544	0.1365	1.837	0.4647

As table 2 shows, compared with locating by only accelerometer, the improved UKF localization algorithm with ultrasonic distance information has higher accuracy.

Estimation of the yaw angle is shown in Fig18. Add white noise whose variance is 0.1 to input yaw angular velocity, the true yaw Angle keep 45 ° firstly, and then increase at a speed of 0.3 rad/s, then decreases at a speed of 0.2 rad/s, as the red curve shows in Fig 18. The blue curve represents the estimation results of the yaw angle, while the black curve represents the estimation of the yaw angle only by the integration of gyroscope. By comparing the errors of the two curves in Fig 19, it is clear that the yaw Angle corrected by the ultrasonic observation overcomes the drift of gyroscope.

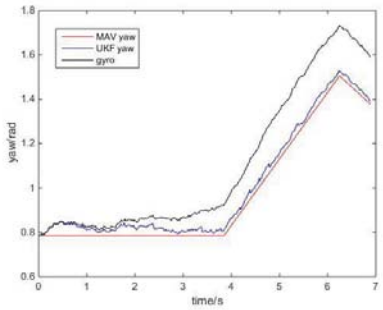

Fig 18 yaw angle result with verifying the validity of observation

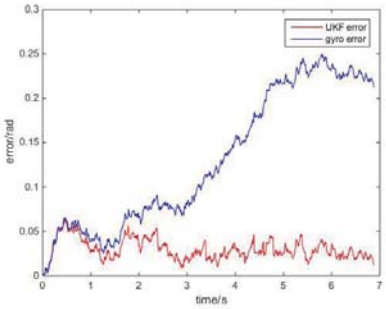

Fig 19 comparison of yaw angle error with improved UKF and with only gyroscope

Table 3 compares yaw estimation error obtained only by gyroscope and by improved UKF. Because the gyroscope has zero deviation, the accumulated error get bigger with time.

As can be seen from table 3, UKF eliminates the influence of the zero deviation of the gyroscope, and the maximum and average error of yaw angle after correction of ultrasonic observation are both smaller than the error integrated by gyroscope.

Table 3 comparison of yaw angle error between two algorithms

Average yaw angle error by gyroscope (rad)	Average yaw angle error by UKF (rad)	Max yaw angle error by gyroscope (rad)	Max yaw angle error by UKF (rad)
0.1307	0.0297	0.2502	0.0628

6 Conclusion

This paper proposes a new indoor localization algorithm based on UKF, which can achieve a more accurate indoor localization effect through four ultrasonic and IMU on-board sensors. The yaw angle can be estimated effectively, even if it changes greatly.

To conclude, because the discontinuous of state equation and observation equations, namely, causing the ultrasonic measurement jump, so in unscented transformation, the range of sampling points could cause a great difference to observation estimation, so UKF is improved in this paper. The localization algorithm adopts different parameters in the process of estimation the state and observation to guarantee observation sampling to keep in a smaller range.

Besides, validity of the measurement is verified, avoiding effect from the observation.

Subsequent work is to apply the algorithm to the real MAV embedded platform to realize the localization function of the algorithm.

References

[1] Kumar, G.A.; Patil, A.K.; Patil, R.; Park, S.S.; Chai, Y.H. A LiDAR and IMU Integrated Indoor Navigation System for UAVs and Its Application in Real-Time Pipeline Classification. Sensors 2017, 17, 1268.

[2] Hélène Roggeman, Julien Marzat, Martial Sanfourche, Aurélien Plyer. Embedded vision-based localization and model predictive control for autonomous exploration. IROS Workshop on Visual Control of Mobile Robots (ViCoMoR 2014), Sep 2014, Chicago, United States. pp.13-20, 2014.

[3] J. Unicomb, R. Ranasinghe, L. Dantanarayana and G. Dissanayake, "A Monocular Indoor Localiser Based on an Extended Kalman Filter and Edge Images from a Convolutional Neural Network," 2018 IEEE/RSJ International Conference on Intelligent Robots and Systems (IROS), Madrid, Spain, 2018, pp. 1-9.

[4] H. Liu, F. Sun, B. Fang and X. Zhang, "Robotic Room-Level Localization Using Multiple Sets of Sonar Measurements," in IEEE Transactions on Instrumentation and Measurement, vol. 66, no. 1, pp. 2-13, Jan. 2017.

[5] D. Hauschildt and N. Kirchhof, "Improving indoor position estimation by combining active TDOA ultrasound and passive thermal infrared localization," 2011 8th Workshop on Positioning, Navigation and Communication, Dresden, 2011, pp. 94-99.

[6] A. Marquez, B. Tank, S. K. Meghani, S. Ahmed and K. Tepe, "Accurate UWB and IMU based indoor localization for autonomous robots," 2017 IEEE 30th Canadian Conference on Electrical and Computer Engineering (CCECE), Windsor, ON, 2017, pp. 1-4.

[7] Stojkoska B R, Palikrushev J, Trivodaliev K, et al. Indoor localization of unmanned aerial vehicles based on RSSI[C]// IEEE Eurocon 2017 - International Conference on Smart Technologies. IEEE, 2017.

[8] Choi J S, Son B R, Kang H K, et al. Indoor localization of Unmanned Aerial Vehicle based on passive UHF RFID systems[C]// International Conference on Ubiquitous Robots and Ambient Intelligence. IEEE, 2013:188-189.

[9] R. Zhang, F. Hoflinger and L. Reindl, "Inertial Sensor Based Indoor Localization and Monitoring System for Emergency Responders," in IEEE Sensors Journal, vol. 13, no. 2, pp. 838-848, Feb. 2013.

[10] Q. Xie, L. Yang and X. Yang, "Micro aerial vehicle indoor localization using prior map and spare sonars," 2017 36th Chinese Control Conference (CCC), Dalian, 2017, pp. 5534-5538.

[11] T. N. Yap and C. R. Shelton, "SLAM in large indoor environments with low-cost, noisy, and sparse sonars," 2009 IEEE International Conference on Robotics and Automation, Kobe, 2009, pp. 1395-1401.

[12] X. Shu, L. Yang and X. Feng, "An IMU/Sonar-based Extended Kalman Filter for Mini-UAV Localization in Indoor Environment, "2018 IEEE/CSAA Guidance, Navigation and Control Conference, Xiamen, 2018.

[13] MB1222 I2CXL-MaxSonar-EZ2 Product Description. [EB/OL]. https://www.maxbotix.com/Ultrasonic_Sensors/MB1222.htm,2019-1-17.

[14] ZHU Y H, LIU J Y, ZENG Q H. Application of state chi-square test in damping Kalman filter of inertial attitude and heading reference system[J]. Chinese Journal of Scientific Instrument, 2007:28(9):1570-1575.

[15] HAUSCHILD T, JENTSCHEL M. Comparison of maximum likelihood estimation and chi-square statistics applied to counting experiments[J]. Nuclear Instruments & Methods in Physics Research, 2001,457:384-401.